Experimental Eye Research 177 (2018) 55–64

Contents lists available at ScienceDirect

Experimental Eye Research

journal homepage: www.elsevier.com/locate/yexer

Retinal structure and function in monkeys with fetal alcohol exposure

Joseph Bouskila[a,b,c,*], Roberta M. Palmour[a,b], Jean-François Bouchard[c], Maurice Ptito[c,d]

[a] Departments of Psychiatry and Human Genetics, McGill University, Montreal, QC, Canada
[b] Behavioral Science Foundations, Saint Kitts and Nevis
[c] School of Optometry, University of Montreal, Montreal, Quebec, Canada
[d] Department of Nuclear Medicine, University of Southern Denmark, Odense, Denmark

ARTICLE INFO

Keywords:
Fetal Alcohol exposure
Monkeys
Intraocular pressure
Electroretinography
Western blots
Immunohistochemistry
Histology
Fundus
Astrocytes
Cone photoreceptors

ABSTRACT

Exposure to ethanol *in utero* leads to several brain development disorders including retinal abnormalities whose underlying cellular pathogenesis remains elusive. We recently reported that fetal alcohol exposure (FAE) in vervet monkeys induces anomalies of full-field electroretinogram (ERG) waveforms that suggest premature aging of the retina. The goal of this study is to characterize the anatomo-functional mechanisms underlying the retinal changes observed in fetal alcohol exposed (FAE) monkeys, and age- and sex-matched normals. First, we examined *in vivo* the fundus of the eyes, measured intraocular pressure (IOP) and assessed cone activity using flicker ERG. Second, we investigated *ex vivo*, protein expression and anatomical organization of the retina using Western blotting, classical histology and immunohistochemistry. Our results indicated that the fundus of the eyes showed both, increased vascularization (tessellated fundus) and IOP in FAE monkeys. Furthermore, light-adapted flicker responses above 15 Hz were also significantly higher in FAE monkeys. Although there were no obvious changes in the overall anatomy in the FAE retina, Glial Fibrillary Acidic Protein (GFAP, a potent marker of astrocytes) immunoreactivity was increased in the FAE retinal ganglion cell layer indicating a strong astrogliosis. These alterations were present in juvenile (2 years old) monkeys and persist in adults (8 years old). Moreover, using specific cell type markers, no significant modifications in the morphology of the photoreceptors, horizontal cells, bipolar cells, and amacrine cells were observed. Our data indicate that FAE does indeed induce anatomical changes within the retinal ganglion cell layer that are reflected in the increased photosensitivity of the cone photoreceptors.

1. Introduction

Exposure to ethanol *in utero* is recognized as one of the leading causes of preventable developmental disorders (Riley and McGee, 2005). The prevalence of neurodevelopmental disorders caused by alcohol consumption during pregnancy is progressively increasing in the World (Tenenbaum et al., 2016). In animal models and humans with fetal alcohol syndrome disorder (FASD), exposure to high or binge levels of alcohol during early pregnancy often lead to neurological, craniofacial, skeletal, cardiovascular, or cognitive-behavioural deficits (Murawski et al., 2015). The more common non-dysmorphic alcohol-related neurodevelopmental disorders are epidemiologically a much greater cause of mild mental retardation in the industrialized world (Roozen et al., 2016). Although many women who drink heavily during pregnancy do not have children with apparent FASD, childhood psychopathology is more common in children with any ethanol exposure during embryogenesis (Coles, 2011). FASD typically presents itself in childhood as learning problems or hyperactivity, or in adolescence as truancy, delinquency, educational failure, and affective disturbances (e.g. impulsivity, loss of control) (Popova et al., 2016).

Fetal alcohol exposure (FAE) can alter the interaction between neurons and glial throughout the central nervous system (CNS) (Evrard et al., 2003). Although Glial Fibrillary Acidic Protein (GFAP) appears to play an important role in the normal development of the CNS, the effects of FAE on GFAP expression are elusive. Interestingly, other glial cells, such as S100b, can induce GFAP expression and increase astrocyte branching (Reeves et al., 1994; Evrard et al., 2006), modulate synaptic plasticity, and affect neuronal and astroglial metabolic pathways (Donato, 2003). Astrocytes also play a role in synaptic pruning (Vecino et al., 2016). In adult rats, FAE causes astrogliosis in the neocortex

Abbreviations: electroretinogram, ERG; fetal alcohol exposure, FAE; fetal alcohol syndrome disorder, FASD; Glial Fibrillary Acidic Protein, GFAP; intraocular pressure, IOP; retinal ganglion cells, RGC

* Corresponding author. Department of Psychiatry and Human Genetics, McGill University, 1033, Pine Ave W, Suite 410, Montreal, Quebec, H3A 1A1, Canada.
E-mail address: joseph.bouskila@mail.mcgill.ca (J. Bouskila).

https://doi.org/10.1016/j.exer.2018.07.027
Received 14 May 2018; Received in revised form 24 July 2018; Accepted 26 July 2018
Available online 30 July 2018
0014-4835/

(Fakoya, 2005). In addition, FAE alters motor behavior and neuroglia in adolescent rats (Brolese et al., 2014). Blood alcohol concentrations in humans of > 100 mg/dl are associated with higher glial protein levels (Brin et al., 2011). Recently, high levels of GFAP in the vitreous humor of patients with retinal diseases was found (Junemann et al., 2015).

The normal and developing retina and visual system are affected by alcohol in many species (Lewis et al., 1970; Sulik and Johnston, 1983; Chmielewski et al., 1997; Tenkova et al., 2003; Kashyap et al., 2007; Dursun et al., 2011; Deng et al., 2012; Lantz et al., 2014). The eye, for example, is a sensitive and reliable marker of alcohol induced abnormalities. These include short palpebral fissures, epicanthus, ocular hypertelorism, coloboma, strabismus, blepharoptosis, microphthalmia, optic nerve head hypoplasia, and irregular vascular tortuosity of the retina (Abdelrahman and Conn, 2009). These aberrations occur in over 90% of FAS children (Stromland, 1985; Stromland, 1987). Cataracts have also been occasionally reported in FAS children (Hanson et al., 1976). However, these cases stem from severe exposure and little is known about the effects of FAE on the retina (Stromland and Pinazo-Duran, 2002). Anatomical changes have been observed in the ventral layers of the primary visual thalamic relay, namely the dorsal lateral geniculate nucleus (Papia et al., 2010). Other parts of the brain are also affected in FAE and decreased neuronal populations have been reported in the hippocampus, olfactory bulb, and dentate gyrus (Burke et al., 2015, 2016).

The full-field or Ganzfeld electroretinogram (ERG) measures retinal function objectively. It records changes in electrical currents across the various retinal cells. The 30 Hz full-field flicker ERG, on the other hand, selectively measures cone-mediated responses, given that rod photoreceptors do not respond at this rate. Most of the studies looking at the effects of FAE on ERG recordings have used either full-field or pattern ERGs to measure the global retinal response (Chan et al., 1991; Hug et al., 2000; Harrar et al., 2017). The goal of this study was two-fold: 1) to characterize the effects of FAE on the retina of vervet monkeys through histology and immunohistochemistry; 2) investigate their consequences on the ERG by selectively targeting the retinal cone system.

2. Material and methods

2.1. Animals

Fifty vervet monkeys (*Chlorocebus sabaeus*) were used: 29 for ERG recordings (10 normals and 19 FAE), and 21 for the anatomical analysis (11 normals and 10 FAE) (Table 1). The monkeys came from the Behavioural Sciences Foundation (St.-Kitts, Eastern Caribbean), and studied under protocols approved by the University of Montreal and the Behavioural Science Foundation, all acting under the auspices of the Canadian Council on Animal Care (CCAC). The animals were fed with primate chow (Harlan Teklad High Protein Monkey Diet; Harlan Teklad, Madison, WI, USA) and fresh local fruits, with water available ad libitum, and lived in outdoor social groups throughout their lives. No animals were euthanized solely for the experiments reported here.

The description of the FAE model has been described in our previous publications (Burke et al., 2016; Harrar et al., 2017). Briefly, following screening for voluntary ethanol consumption, alcohol-preferring adult females were housed in small breeding groups with a matched-aged alcohol-avoiding male. The groups were monitored behaviorally for reproductive activity. Females were then examined twice a week to identify gestational age. Alcohol (range 1.2–5.51 g of alcohol/kg body weight/day; 10% v/v solution presented in a calibrated drinking bottle) began at about embryonic day 95 of the 165-day gestation period for vervet monkeys. Tap water was always concurrently available. To avoid withdrawal periods, alcohol was available 4 days per week for a 4-h period in individual compartments close to their social groups. At the time of birth, alcohol exposure was terminated.

Table 1
Animals' profile.

	Animal	Sex	Weight (Kg)	Av Alc (g/kg/day)	Group	Experiment
1	O1593-4-1-8	male	2.70	0	ctrl	ERG
2	O1659-2-6-7	male	2.34	0	ctrl	ERG
3	O2244-1-1-2-3	male	2.32	0	ctrl	ERG
4	O2301-7-9	female	1.89	0	ctrl	ERG
5	O2785-2-9	male	2.36	0	ctrl	ERG
6	O3087-1-2-2	female	2.00	0	ctrl	ERG
7	O4011-1-2-3	male	2.02	0	ctrl	ERG
8	O8711-7-1-7	female	1.95	0	ctrl	ERG
9	O9150-8-5	male	2.15	0	ctrl	ERG
10	O9184-4-8	male	2.50	0	ctrl	ERG
11	N1007-4-1-1-7	female	2.78	1.2	FAE	ERG
12	N1007-4-1-1-8	male	2.37	2.21	FAE	ERG
13	N454-5-2-6-2	male	2.82	2.15	FAE	ERG
14	N459-1-15-3	male	2.76	2.1	FAE	ERG
15	N459-1-9-7-1	female	2.60	2.49	FAE	ERG
16	O1344-1-1-6-1	male	2.41	3.01	FAE	ERG
17	O1645-1-5-6	male	2.53	4.05	FAE	ERG
18	O1720-4-3-3-2	male	2.30	3.09	FAE	ERG
19	O1731-2-2-3-6	female	2.45	2.09	FAE	ERG
20	O1873-5-7-2	male	3.07	2.18	FAE	ERG
21	O2301-7-3-1	male	2.45	3.08	FAE	ERG
22	O2334-7-6	male	2.38	2.47	FAE	ERG
23	O2659-1-6-2	female	2.29	5.51	FAE	ERG
24	O3263-3-6	male	2.05	2.86	FAE	ERG
25	O3284-7	male	1.97	2.62	FAE	ERG
26	O3372-9	female	2.83	3.45	FAE	ERG
27	O8711-7-7	male	3.20	2.23	FAE	ERG
28	O8711-8-6-1	male	3.14	3.11	FAE	ERG
29	O8711-8-6-2	female	2.58	3.51	FAE	ERG
30	O1198-3-10	female	3.75	0	ctrl	WB
31	O9010-11	female	3.67	0	ctrl	WB
32	O9180-5-1	male	6.05	0	ctrl	WB
33	O3066-3	female	4.55	2.1	FAE	WB
34	O3372-3	male	6.35	3.25	FAE	WB
35	O5335-2	female	4.30	2.5	FAE	WB
36	O1842-4-1	male	6.08	0	ctrl	IF
37	O1873-2-6-1	male	2.31	0	ctrl	IF
38	O2251-1-2-1	female	4.06	0	ctrl	IF
39	O3345-3	female	2.48	0	ctrl	IF
40	O4020-6	male	2.52	0	ctrl	IF
41	O4026-7	female	2.00	0	ctrl	IF
42	O4026-7	female	2.63	0	ctrl	IF
43	O5151-1	male	2.01	0	ctrl	IF
44	O3327-2	female	2.77	3.3	FAE	IF
45	O1669-3-7	female	3.99	3.28	FAE	IF
46	O3372-4	female	4.31	2.59	FAE	IF
47	O5330-3	female	4.13	3.04	FAE	IF
48	O5332-1	female	2.05	2.19	FAE	IF
49	O5892-1	female	4.74	2.54	FAE	IF
50	O5892-1	female	4.74	3.14	FAE	IF

2.2. In vivo animal preparation

The monkeys were anesthetized with an intramuscular injection of ketamine (10 mg/kg) and xylazine (1 mg/kg) as previously described (Bouskila et al., 2014, 2016a, 2016b). The pupils were then fully dilated with 1% tropicamide and 2.5% phenylephrine hydrochloride. Proparacaine hydrochloride (0.5%) was used for local anesthesia and methylcellulose (2.5%) to prevent corneal drying.

2.3. Ophthalmological evaluation

Under sedation and mydriasis, clinical examination (direct ophthalmoscopy and IOP) was performed. We observed the fundus of the eyes using the panoptic ophthalmoscope (Welch Allyn, Skaneateles Falls, NY, USA) attached to an iPhone camera (iExaminer, Welch Allyn, Skaneateles Falls, NY, USA) for pictures taking and examined IOP with the applanation tonometer (TonoPen XL; Mentor, Norwell, MA, USA).

Table 2
List of antibodies.

Antibody[a]	Immunogen	Source[b]	Working dilution	MW (kDa)
ALDH1L1	Recombinant full-length rat Aldh1L1	Mouse monoclonal, Clone N103/39, EMD Millipore Corporation, MABN495, AB_2687399	I: 1:150 W: 1:500	99
Brn3a	Amino acids 186-224 of Brn3a protein	Mouse monoclonal, EMD Millipore Corporation, MAB1585, AB_94166	I: 1:50 W: 1:500	46
Calbindin	Recombinant protein specific to the amino terminus of human calbindin protein	Rabbit monoclonal, Clone D1|4Q, Cell Signaling, 13176, AB_2687400	I: 1:200 W: 1:1000	28
CHX10	Recombinant human CHx10 protein, N-terminal	Sheep polyclonal, EMD Millipore Corporation, AB9016, AB_2216009	I: 1:50 W: 1:1000	46
GAPDH	The full-length rabbit muscle GAPDH protein	Mouse polyclonal, Sigma-Aldrich, G8795, AB_1078991	W: 1:5000	37
GFAP	Synthetic peptide corresponding to residues surrounding Asp395 of human GFAP protein	Rabbit monoclonal, Clone D1F4Q, Cell Signaling, 12389, AB_2631098	I: 1:200 W: 1:1000	50
GS	Full protein purified from sheep brain	Mouse monoclonal, Clone GS-6, EMD Millipore Corporation, MAB302, AB_2110656	I: 1:200 W: 1:1000	45
PKCα	Epitope mapping between amino acids 645-672 at the C-terminus of PKCα of human origin	Mouse monoclonal, Clone H-7, Santa Cruz Biotechnology, sc-8393, AB_628142	I: 1:200 W: 1:1000	80
PV	Parvalbumin purified from carp muscles	Mouse monoclonal, Swant, 235, AB_10000343	I: 1:200 W: 1:1000	12
RBPMS	KLH-conjugated linear peptide corresponding to a sequence from the N-terminal region of human RBPMS	Guinea pig polyclonal, EMD Millipore Corporation, ABN1376, AB_2687403	I: 1:100 W: 1:500	25
Syntaxin	Synaptosomal plasma fraction of rat hippocampus[c]	Mouse monoclonal, Clone HPC-1, Sigma-Aldrich, S0664, AB_477483	I: 1:200 W: 1:1000	35
Vimentin	Synthetic peptide corresponding to residues surrounding Arg45 of human vimentin protein	Rabbit Monoclonal, Clone D21H3, Cell Signaling Technology, 5741, AB_10695459	I: 1:100 W: 1:1000	57
Alexa Fluor 488 donkey anti-mouse	Mouse Gamma Immunoglobins Heavy and Light chains	Donkey polyclonal, Invitrogen, A-21202, AB_141607	I: 1:200	N/A
Alexa Fluor 488 donkey anti-rabbit	Rabbit Gamma Immunoglobins Heavy and Light chains	Donkey polyclonal, Invitrogen, A-21206, AB_2535792	I: 1:200	N/A
Alexa Fluor 647 donkey anti-mouse	Mouse Gamma Immunoglobins Heavy and Light chains	Donkey polyclonal, Invitrogen, A-31571, AB_162542	I: 1:200	N/A
Alexa Fluor 647 donkey anti-rabbit	Rabbit Gamma Immunoglobins Heavy and Light chains	Donkey polyclonal, Invitrogen, A-31573, AB_2536183	I: 1:200	N/A
Alexa Fluor 647 donkey anti-guinea pig	Guinea Pig Gamma Immunoglobins Heavy and Light chains	Donkey polyclonal, EMD Millipore Corporation, AP193SA6, AB_2629452	I: 1:200	N/A

[a] Abbreviations: GAPDH, Glyceraldehyde-3-Phosphate Dehydrogenase; GFAP, glial fibrillary acidic protein; GS, glutamine synthetase; I, immunohistochemistry; MW, molecular weight; PV, parvalbumin; RBPMS, RNA-binding protein with multiple splicing; W, Western blot.
[b] The source column indicates the host species, commercial company, catalog reference and RRID. The clone designation is given for monoclonal antibodies when available.
[c] See Barnstable et al., 1985.

2.4. Quantification of retinal layer thickness

The quantification of the thickness of all layers of the central retina was performed as previously described by our group (Cecyre et al., 2013). Briefly, after washing frozen retinal sections in 0.1M PBS, the nuclei were labeled with Sytox Green Nucleic Acid Stain (1:10,000; Molecular Probes, Eugene, OR, USA) for 10 min. The images of the central retina were taken at 40× magnification, including the outer nuclear layer (ONL), the outer plexiform layer (OPL), the inner nuclear layer (INL), the inner plexiform layer (IPL), and the ganglion cell layer (GCL). The thickness of each layer was measured with ImageJ software (developed by US National Institutes of Health). We corrected for local and inter-animal variations. Statistical analysis was performed by using one-way ANOVA.

2.5. Visual stimulation

Electroretinogram responses were recorded from both eyes using the UTAS E-3000 electrophysiology equipment (LKC Technologies, Inc., Gaithersburg, MD, USA). Using a steady white background-adapting field (30 cd/m^2) presented inside the Ganzfeld to saturate the rod system, ERGs were evoked by a flicker LED flash luminance of 2.57 cd s m^2 (0.4 log cd.s.m^2) delivered in full-field conditions. The flash intensity and background luminance were calibrated using the IL1700 research radiometer equipped with a SED033 detector.

2.6. Flicker ERG recording and analysis

Light-adapted flicker ERG was used to specifically target cone function. The experimental protocol followed the recommendations of the ISCEV, including the light-adapted response to a rapidly repeated stimulus (30 Hz flicker). ERG recordings and signal processing were recorded with contact lens electrodes lying across the center of the cornea of each eye moistened with 1% carboxymethylcellulose sodium. The corneal contact lens electrode was equipped with four small posts on the convex surface in order to keep the eyelids open. Reference and ground gold disc electrodes were kept in place with adhesive paste at the external canthi and forehead, respectively. The amplitudes and timing values were extracted with the LKC software. Up to 10 waveforms were averaged to reduce variability and background noise.

2.7. Tissue preparation

After sedation, the animals were deeply anesthetized with sodium pentobarbital (25 mg/kg, i. v.), and perfused transcardially with phosphate-buffered saline (PBS 0.1 M; pH 7.4). One eye was immediately fixed, and the other eye had its retina dissected out and immediately frozen. For immunohistochemistry, one eyeball was fixed in 4% paraformaldehyde. Fixed retinas were then dissected free from the eye in a phosphate buffered saline bath. The retina was laid flat so that the vitreous body could be removed by blotting with filter paper and gentle brushing (Burke et al., 2009a,b; Bouskila et al., 2012, 2013a, 2013b).

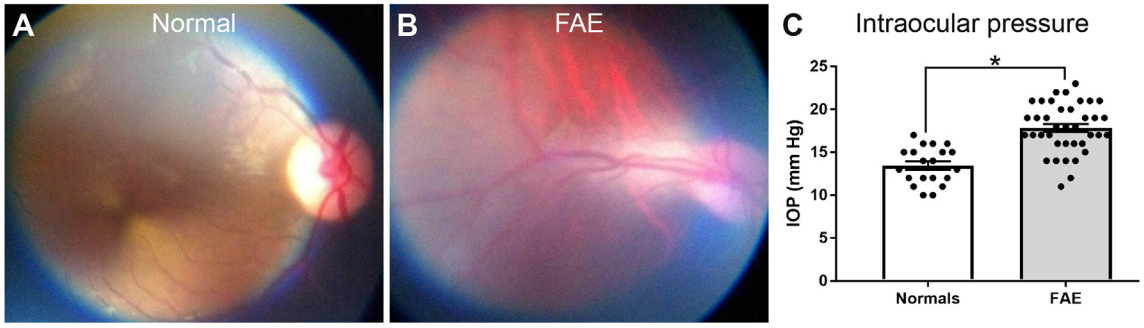

Fig. 1. Ophthalmologic manifestations of moderate fetal alcohol exposure. Typical fundus photograph obtained in a normal monkey (**A**) and a FAE monkey (**B**). Assessment of IOP with individual values (**C**).

Tissue samples were taken from the optic nerve, optic disk and central retina, and then cryoprotected in 30% sucrose overnight and embedded in Shandon embedding media. Sections of 25 µm were mounted on gelatinized slides and stored at −20 °C. For Western Blotting, the retinas were dissected free from fresh eyeballs and stored at −80 °C.

2.8. Western blot

Frozen retinal tissue was homogenized by hand using a sterile pestle in a radioimmunoprecipitation assay buffer (150 mM NaCl, 20 mM Tris, pH 8.0, 1% NP-40, 0.1% sodium dodecyl sulfate (SDS), 1 mM EDTA), supplemented with protease inhibitors (Pierce Protease Inhibitor Tablets #88266, Thermo Fisher Scientific, Rockford, IL, USA) and phenylmethylsulfonyl fluoride (0.2 mg/ml; Roche Applied Science, Laval, QC, Canada). Samples were then centrifuged at 4 °C for 10 min, and the supernatant was extracted and stored at −20 °C until further processing. Protein content was equalized using a Thermo Scientific Pierce BCA Protein Assay Kit (Fischer Scientific, Ottawa, ON, Canada). Fifteen micrograms of protein/sample of the homogenate were resolved with 10% SDS-polyacrylamide gel electrophoresis, transferred onto a nitrocellulose membrane filter (BioTrace NT, Life Sciences, Pall, Pensacola, FL, USA), blocked for 1 h in 5% skim milk (Carnation, Markham, ON, Canada) in TBST (0.15 M NaCl, 25 mM Tris–HCl, 25 mM Tris, 0.5% Tween-20), and incubated overnight with primary antibodies (Table 2) in blocking solution. The following day, the blot was exposed to a secondary antibody conjugated to horseradish peroxidase (1:5000; Jackson ImmunoResearch, West Grove, PA, USA) in blocking solution for 2 h. Detection was carried out by using home-made enhanced chemiluminescence Western blotting detection reagents (final concentrations: 2.50 mM luminol, 0.4 mM *p*-coumaric acid, 0.1 M Tris-HCl pH 8.5, 0.018% H_2O_2). The membrane was then air-stripped, re-blocked, and exposed to a second primary antibody, namely mouse anti-GAPDH (1:20,000), until all proteins of interest were tested.

2.9. Immunofluorescence

Single, double and triple labeling of the retina tissue was performed according to previous published methods on vervet monkey retina (Bouskila et al., 2012; Bouskila et al., 2013a, 2013b; Bouskila et al., 2016a, 2016c). Briefly, sections were rinsed 3 × 5 min in Tris 0.1 M buffer, pH 7.4/Triton 0.03%, and blocked for 90 min in 10% normal goat serum (NDS) in Tris 0.1 M buffer/0.5% Triton. Sections were incubated overnight at 4 °C temperature with primary antibodies in blocking solution. The GFAP antibodies were used with specific retinal cell markers (Table 2). The following day, sections were washed for 10 min and 2 × 5 min in Tris 0.1 M/Triton 0.03%, blocked in 10% NDS, Tris 0.1 M/0.5% Triton for 30 min, and incubated with a secondary antibody for 1 h all in blocking solution (Table 2). Sections were washed again in Tris buffer, counterstained with Sytox Orange nucleic acid stain (Life Technologies, Eugene, OR, USA), and coverslipped with Fluoromount-G™ Mounting Medium (SouthernBiotech, Birmingham, AL, USA).

2.10. Confocal microscopy

Immunofluorescence images were taken as previously described (Bouskila et al., 2012; Bouskila et al., 2016a). A Leica TCS SP2 confocal laser-scanning microscope (LeicaMicrosystems, Exton, PA, USA), equipped with a 40× (n.a.: 1.25) and a 100× (n.a: 1.40–0.7) objective, was used to obtain sequential images from the green, blue, and far-red channels. Image adjustments were done with Adobe Photoshop (CC, Adobe Systems, San Jose, CA, USA) and then exported to Adobe In-Design (CC, Adobe Systems, San Jose, CA, USA) for final figure layout.

3. Results

3.1. Ophthalmoscopy and intraocular pressure (IOP)

All vervet monkeys displayed optic nerve heads that were vertically oval, similar to what is observed in macaque monkeys (Fig. 1A) (Wolin and Massopust, 1967; Malinow et al., 1980). The disks were of normal color in all animals. Tessellated fundi were found in many FAE monkeys (Fig. 1B). Normal and FAE monkeys had IOP measures within the normal range (12–22 mm Hg). However, the IOP of the FAE monkeys was significantly higher than normal animals (*t*-test, $p < 0,01$) (Fig. 1C).

3.2. Flicker electroretinogram (ERG)

The photopic flicker ERG was recorded in normal and FAE monkeys at 10 different frequencies, ranging from 5 Hz to 50 Hz, obtained in light-adapted conditions (30 cd m^2) with standard intensity light flashes (2.57 cd s m^2). At frequencies of 15 Hz and above, the amplitude was significantly higher in FAE monkeys compared to normals (repeated measures ANOVA, $p < 0,01$) (Fig. 2A). There was no significant difference in implicit time values between the two groups of animals (Fig. 2B). Fig. 2C shows raw flicker ERG traces in normal and FAE monkeys.

3.3. Retinal structure in FAE monkeys

To analyze structural changes in FAE monkeys, we compared their basic retinal anatomy with normal monkeys by examining retinal layering and thickness. The typical retinal layering appeared normal in our 2 groups (Fig. 3A). Visual inspection of the retinas showed no obvious changes in retinal structures. We then assessed layer thickness as

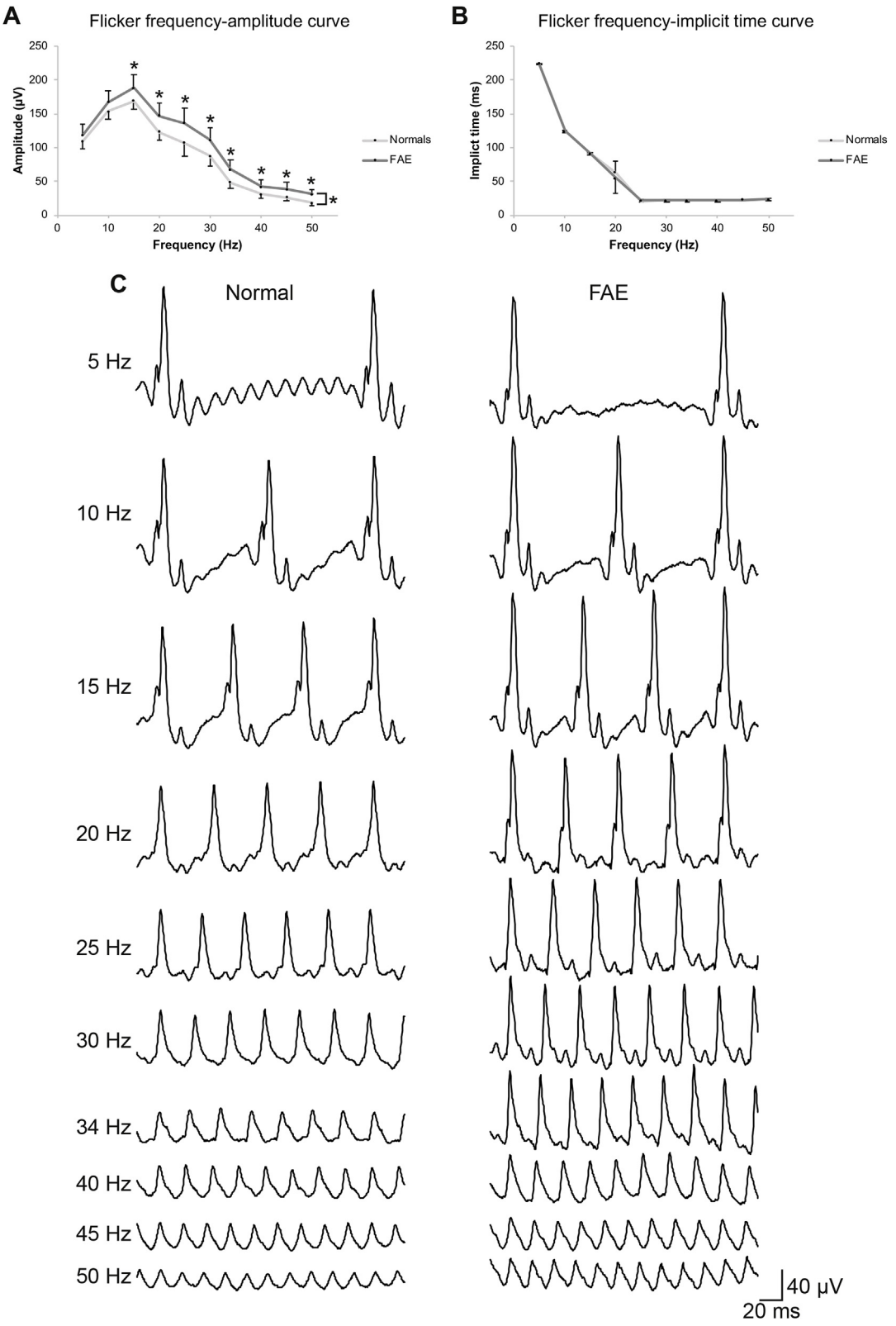

Fig. 2. Frequency-response relationship of the flicker ERG. Responses were elicited at 10 different flicker frequencies. Flash intensity was constant at 2.57 cd s m^{-2}. Peaks in amplitude values were observed at 15 Hz (**A**). Implicit times decreased with increasing frequency values (**B**). Data was averaged from 10 normal monkeys (white) and 19 FAE monkeys (grey). Raw flicker ERG traces in representative normal (left) and FAE (right) monkeys at 10 different frequencies (5 Hz, 10 Hz, 15 Hz, 20 Hz, 25 Hz, 30 Hz, 34 Hz, 40 Hz, 45 Hz, 50 Hz) (**C**). Scale is given by the inserts.

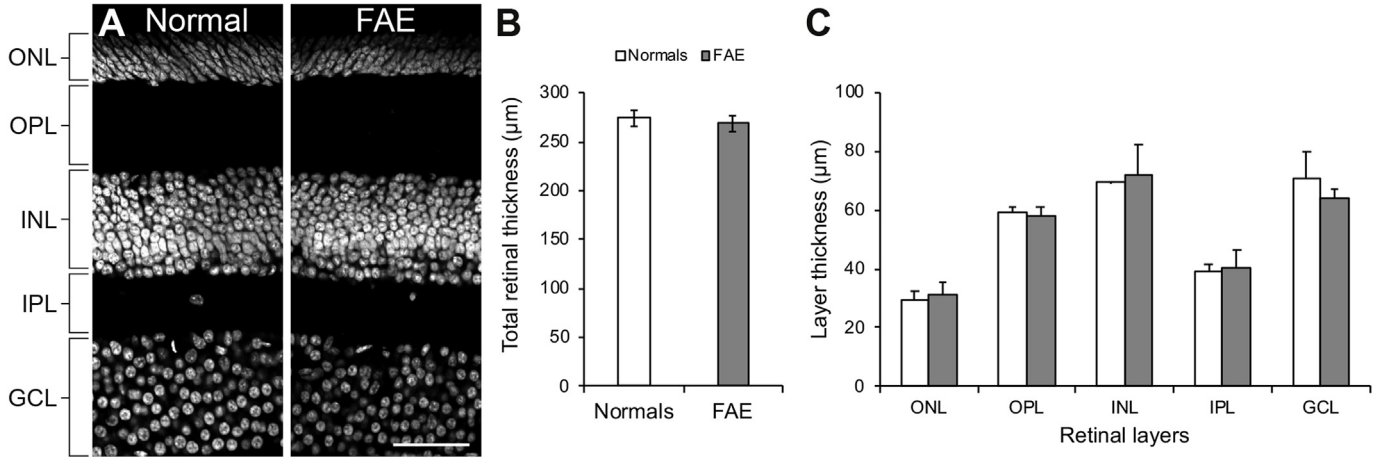

Fig. 3. No change of basic retinal morphology in FAE monkeys. (**A**) Nuclei staining of retinas of normal and FAE monkeys with Sytox. Normal retinal layer structures were preserved in all monkeys. Scale bar = 75 µm. (**B**) Total thickness calculated from ONL-GCL in 3 normal monkeys and 3 FAE monkeys. (**C**) Mean thickness of each retinal layer in the two groups. White bars correspond to normal monkeys and grey bars to FAE monkeys.

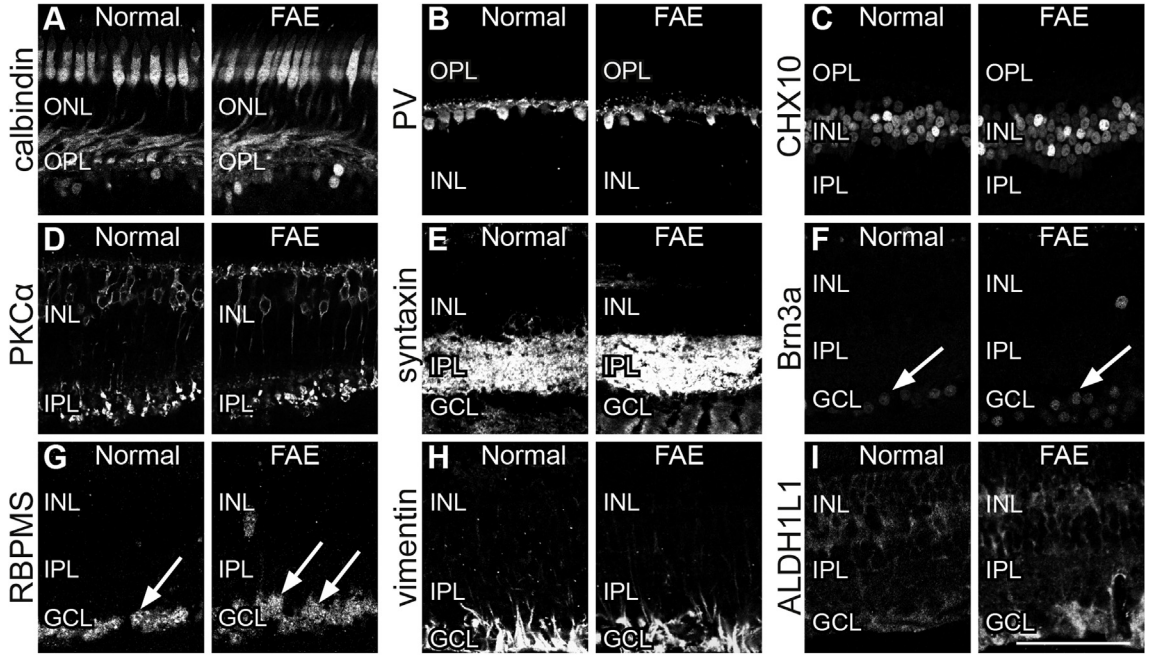

Fig. 4. The FAE retina does not have any obvious changes in the distribution and morphology of cone photoreceptors (calbindin, **A**), horizontal cells (PV, **B**), bipolar cells (CHX10, **C**), rod bipolar cells (PKC, **D**), amacrine cells (syntaxin, **E**), ganglion cells (Brn3a, **F**; RBPMS, **G**), Müller cells (vimentin, **H**; ALDH1L1, **I**). Normal morphology and distribution of every retinal cell types were preserved in both groups. Arrows point at retinal ganglion cell nuclei that are Brn3a- or RBPMS-positive. Scale bars = 75 µm.

a measure of retinal integrity. The total retinal thickness (Fig. 3B) and the thickness of each layer (Fig. 3C) were precisely measured. No significant differences were found for all parameters (total thickness: 274 ± 8 µm in normals, 269 ± 6 µm in FAE, p = 0.60; ONL: 29 ± 3 µm in normals, 31 ± 4 µm in FAE, p = 0.62; OPL: 59 ± 2 µm in normals, 58 ± 3 µm in FAE, p = 0.70; INL: 69 ± 0.3 µm in normals, 72 ± 10 µm in FAE, p = 0.77; IPL: 39 ± 2 µm in normals, 41 ± 6 µm in FAE, p = 0.79; GCL: 71 ± 9 µm in normals, 64 ± 3 µm in FAE, p = 0.40). The overall retinal layering was thus preserved in FAE monkeys. In addition, the distribution and morphology of distinct retinal cells were compared to verify if they were affected. No obvious changes were observed in any retinal cell type in both groups (Fig. 4; see below for details).

3.4. No change in cone photoreceptors

Labeling with calbindin, a specific cone photoreceptor cell marker outside the foveola, allowed us to distinguish the morphology of cone photoreceptors (Fig. 4A). Our results show that extrafoveal cone photoreceptors, including the cone outer segments, are similar in shape in FAE and normal monkeys (Fig. 4A). In all FAE retinas, we found the same staining pattern. No differences in the expression of calbindin

were observed throughout the outer/inner segments, cell body and terminals.

3.5. No change in horizontal cells

Labeling with parvalbumin, a specific horizontal cell marker, allowed us to highlight the absence of change in horizontal cell morphology and distribution (Fig. 4B).

3.6. No change in bipolar cells

Labeling of CHX10, a bipolar cell nucleus marker, allowed the demonstration that bipolar cell nuclei were similarly distributed in both FAE and normals (Fig. 4C). Labeling of PKC, a rod bipolar cell marker, established that rod bipolar cell dendritic fibers juxtaposed to rod spherules were similar in both groups (Fig. 4D).

3.7. No change in amacrine cells

The monoclonal antibody HPC-1 that recognizes syntaxin in horizontal and amacrine cells was used to evaluate morphological changes in amacrine cells (Fig. 4E). Despite variations in intensity of immunolabeling in the RGC layer representing axon fiber staining, there was no difference in the thickness of the IPL (Fig. 4E).

3.8. No change in retinal ganglion cells (RGCs)

Brn3a (a transcription factor used to identify RGCs in many species) and RBPMS (RNA-binding protein with multiple splicing; a selective marker of ganglion cells in the mammalian retina) immunoreactivities were used to specifically label retinal ganglion cell nuclei in vervet monkeys. The ganglion cell bodies (arrows) in the monkey central retina were similar in shape in the FAE and normal animals (Fig. 4F and G).

3.9. No change in müller cells

In order to label Müller cells in the monkey retina, the antibodies vimentin and ALDH1L1 were used. Vimentin and ALDH1L1 labels Müller glia end feet in macaque, and in some cases, astrocytes (Fischer et al., 2010). Our results show no difference in the membrane of the Müller cells' soma or in their inner and outer processes (Fig. 4H and I).

3.10. Retinal glia changes in FAE

Furthermore, in order to establish if the retinal glia was affected in FAE animals, we measured the total amounts of 3 different glial proteins, namely, GFAP, ALDH1L1, and vimentin (Fig. 5A). Glial protein expression was assessed by Western blotting in normal and FAE retinas. A more prominent GFAP band with an estimated molecular weight of ~50 kDa was observed in FAE monkey retinas compared to normals. The protein GAPDH (37 kDa) was used to demonstrate equal loading for the Western blotting experiments. The expression of GFAP in each blot was then measured by densitometry and normalized to GAPDH levels. Normalized GFAP expression levels revealed a marked difference between normal and FAE retinas. Expression fold changes were calculated as the ratio between FAE and normal normalized values. Specifically, we observed a 4-fold increase in GFAP expression in the retina of FAE monkeys compared to normal animals ($p < 0,01$, ANOVA followed by Bonferroni's test). This GFAP overexpression in FAE monkey retinas parallels our main result where higher GFAP immunoreactivity is observed in astrocytes of the FAE retina (Fig. 5A and B). No changes were found for ALDH1L1 (Fig. 5C) and vimentin (Fig. 5D).

3.11. Distribution of astrocytes in normal and FAE retinas

To assess astrocyte changes following FAE, the morphology and distribution of retinal astrocytes were studied in normal and FAE retinas through immunocytochemical localization of GFAP. Fig. 6 illustrates the localization of astrocyte projections in retinal sections from normal (Fig. 6A) and FAE (Fig. 6B) monkeys. In normal and FAE retinas, astrocytes processes were mainly distributed in the ganglion cell layer (GCL).

3.12. Cellular localization of GFAP

The GCL is composed of ganglion cells, Müller cells, astrocyte processes, and displaced amacrine cells. Müller cell and astrocyte processes enroll the cell bodies of ganglion cells. We have shown that glutamine synthetase (GS) specifically labels Müller cells in many species, including the vervet monkey retina (Bouskila et al., 2016a). To distinguish between Müller cells and astrocytes, double-labeling of GFAP with GS allowed us to limit gliosis to astrocytes (Fig. 7).

4. Discussion

Previous reports showed that this natural model of FAE in vervet monkeys has systematic and quantitative brain changes in response to alcohol levels commonly observed in a human social context (Burke et al., 2009a,b; Burke et al., 2015, 2016; Papia et al., 2010). In this report, we investigated the functional and anatomical consequences of FAE in the monkey retina. Using flicker ERG recordings, we showed that cone-mediated responses are increased in FAE monkeys. Using

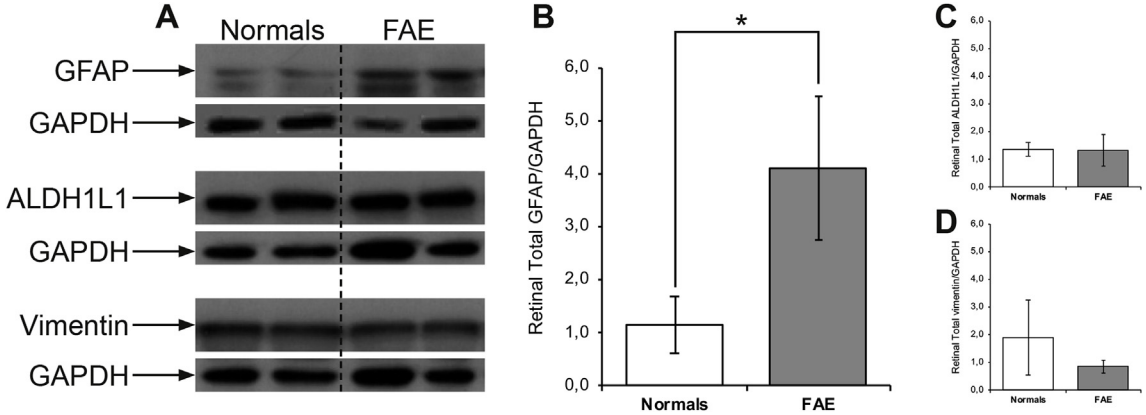

Fig. 5. Western Blots analysis of total protein samples from the retina. Immunoblots of GFAP, ALDH1L1, and vimentin immunoreactivities in normal and FAE monkeys (**A**). The GFAP protein band is increased in the FAE retina (**B**), while ALDH1L1 (**C**), and vimentin (**D**) does not change.

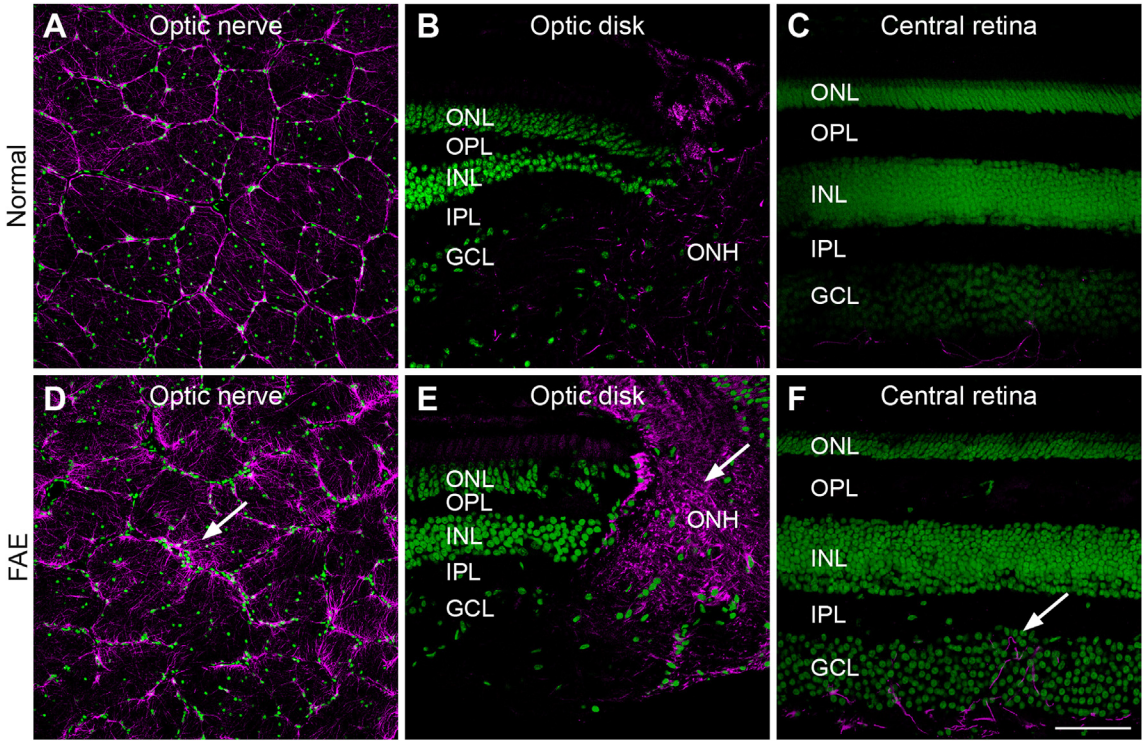

Fig. 6. GFAP immunoreactivity is increased in the FAE optic nerve and retina. Confocal micrographs of vertical sections taken from the optic nerve (**A**, **D**), optic disk (**B**, **E**), and central retina (**C**, **F**) immunolabeled for GFAP and counterstained with Sytox Green (nuclear stain). Arrows point at the increase of GFAP-positive astrocyte projections. Scale bar = 150 μm for A and D, and 75 μm for B, C, E, F. (For interpretation of the references to color in this figure legend, the reader is referred to the Web version of this article.)

immunohistological labeling and immunoblots, we showed that the expression of many different proteins of interest remains constant after birth in FAE monkeys, while that of GFAP is increased in the FAE monkey retina. Our data provide evidence of the increased presence of astrocytes in the inner retina of FAE monkeys.

4.1. Animal model of FAE

Old-World monkeys represent an excellent model for protein expression analysis in this context for two reasons: 1) the anatomy and physiology of the visual system in vervet monkeys, including retina, lateral geniculate nucleus, and primary visual cortex, reflects well what is seen in humans (Chaudhuri et al., 1996; Bouskila et al., 2012); and 2) the differential expression of many proteins in the vervet monkey retina and their relationship to retinal function (Bouskila et al., 2016a, 2016b). Furthermore, the genetic similarity between Old-World monkeys and man is 96–98%, and many conserved proteins have identical sequences. The hypothesis that pre-and perinatal ethanol damage is related to changes in astrocytes has been studied by many groups with, however, contradictory results, some finding an increase of GFAP (Miller and Robertson, 1993; Evrard et al., 2003, 2006; Fakoya, 2005; Brolese et al., 2014), and others, a decrease (Renau-Piqueras et al., 1989; Sáez et al., 1991; Valles et al., 1996, 1997). This discrepancy can be explained, at least in part, by different animal species, different models of ethanol exposure and different developmental time points.

4.2. Increased intraocular pressure and flicker ERG responses

Early studies have reported that acute alcohol consumption decreases IOP by 3.7 mm Hg, regaining normal values after 65 min (Buckingham and Young, 1986). However, two epidemiologic studies reported that chronic alcohol consumption is associated with an increase of IOP (Leske et al., 1996; Wu and Leske, 1997). We do not report here the direct effect of acute or chronic alcohol consumption, but rather the effect of prenatal alcohol consumption on the retina of offspring. While we found that our 2 groups had IOP in the normal range, FAE animals had a statistically significant higher IOP. Interestingly, GFAP expression is increased in response to elevated intraocular pressure in rats and monkeys (Tanihara et al., 1997; Kim et al., 1998). It is therefore reasonable to assume that the higher IOP observed in our

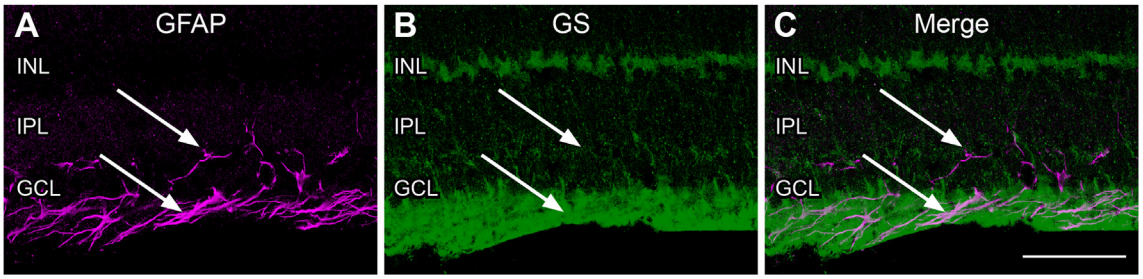

Fig. 7. Double-labeling of GFAP and GS. Labeling of GS-positive Müller cells in the monkey retina did not colocalize with GFAP (magenta). Arrows point at astrocyte projections that are not GS-positive Müller cell fibers. Scale bar = 75 μm.

FAE monkeys is responsible for the increased astroglyosis in the retinal ganglion cell layer. It might also be possible that this abnormal increase in astrocytes in the RGC layer is responsible for the higher photopic flicker ERG amplitudes. Whether these changes impact visual acuity and visual behavior in general remains to be investigated.

4.3. GFAP is increased in the FAE monkey retina

The present results confirm the increased expression of GFAP in the FAE monkey retina. To our knowledge, this study is the first to precisely characterize a retinal protein that is changed after prenatal alcohol consumption. Our laboratories have used the same animal model with the same alcohol exposure paradigm and have found alterations in different regions of the brain, particularly the olfactory bulb (Burke et al., 2009a,b; Burke et al., 2015, 2016). Even though it is becoming clear that astrocytes play an important role in the CNS and reactive astrocytes in CNS injury and disease, the cellular mechanisms initiating reactive astrogliosis is not as yet well defined. What can be definitively said is that there is an extensive molecular repertoire of reactive astrocytes, and these include cytokines, chemokines, and others (see Sofroniew, 2009 for review). There can be many beneficial, as well as, detrimental effects exerted by reactive astrogliosis depending on the context. Reactive astrogliosis appears when there is a loss of normal functions, or when there is a gain in pathological functions that are present in many diseases. Astrogliosis serves as important regulator of inflammatory responses (Sofroniew and Vinters, 2010; Sofroniew, 2015).

FAE induced an increase of GFAP expression in the monkey retina that appeared to come from the optic disk. The accumulation of thick astrocyte processes was frequently observed around small blood vessels in the nerve fiber layer of the FAE retina. Given that these cells highly express GFAP and have thick processes, they fit the criteria of reactive astrocytes. Furthermore, the increase of GFAP was also located in the RGC layer which suggests the presence of hypertrophied astrocyte processes. It is noteworthy to note that the specific mechanisms which initiate glial reactions in pathological conditions are still currently unknown. Nevertheless, when reactive gliosis surrounding retinal vessels occurs, this suggests that FAE may be associated with disruption of the normal development of the blood-retinal barrier. Indeed, reactive gliosis can be induced when the blood-retinal barrier is damaged or in inflammation, probably, in response to the entry of factors that act as mitogens for astrocytes. Early postnatal alcohol exposure (> 150 mg/dl) can produce small focal hemorrhages (Anderson and Sides, 1979; Volk, 1984). High levels of alcohol intake (> 250 mg/dl) can induce severe spasms that result from rupture of the cerebral vasculature (Altura and Altura, 1984). However, the precise molecular signals and mechanisms of action which regulate the blood-retinal barrier development in response to fetal alcohol exposure remain to be assessed and may be multifactorial.

The present results can be extrapolated to humans. Alcohol exposure during the third trimester of pregnancy can induce reactive gliosis and therefore interfere with the normal development of the brain and retina. The increased ERG amplitude in FAE vervets may be the result of a pathological increase due to anomalies of the cerebral and retinal vasculature induced by alcohol. Also, FAE during the third trimester can alter the development of glial cells, such as astrocytes, and modify the expression of GFAP in the retina. This would indicate that alcohol consumption in late pregnancy, when the baby is already formed, is still not safe. It is important to elucidate the specific mechanisms of action initiating the increase of GFAP expression in astrocytes. This will help us understand how alcohol affects normal brain and retinal development during the third trimester. It is well known that reactive astrogliosis in the brain occurs with aging (Sloane et al., 2000). It has been recently hypothesized that premature aging of the visual system may be occurring in FAE vervet monkeys (Harrar et al., 2017). Our results confirm that hypothesis by showing alcohol-associated increases in astrocytic hypertrophy in the retina of vervet monkeys. Here, we propose that the functional changes observed in the FAE retina are not due to abnormal retinal cell distribution (Harrar et al., 2017), but rather to the increase of astrocytes that induce a higher potassium buffering (Reichenbach et al., 1993; Walz, 2000). This assumption is supported by our results that showed an increased photopic flicker ERG amplitudes in FAE monkeys.

Acknowledgements

The authors thank all the staff of the Behavioural Sciences Foundation for their expert technical assistance in handling the monkeys, Ryan Kucera, Mads Lundgaard, and Clara Eid for support with data collection, and Amy Beierschmitt and Heather Hotchin for excellent animal care.

This work was supported by the Natural Science and Engineering Research Council of Canada (6362-2017, Dr Maurice Ptito; RGPAS 478115-2015/RGPIN 2015-06582, Dr Jean-François Bouchard) and Canadian Institutes of Health Research (PJT-156029, Dr Jean-François Bouchard). Dr Joseph Bouskila is supported by a NSERC postdoctoral research award. Dr Jean-François Bouchard was supported by a “Chercheur-Boursier Senior” from the Fonds de recherche du Québec Santé (FRQ-S). Dr Maurice Ptito holds the Harland Sanders Chair in Visual Science. The animal resources on which this paper is based were supported by grants from CIHR (MOP 57899) and generous in-kind support from Behavioural Science Foundation.

References

Abdelrahman, A., Conn, R., 2009. Eye abnormalities in fetal alcohol syndrome. Ulster Med. J. 78, 164–165.
Altura, B.M., Altura, B.T., 1984. Alcohol, the cerebral circulation and strokes. Alcohol 1, 325–331.
Anderson, W.J., Sides, G.R., 1979. Alcohol induced deffects in cerebellar development in the rat. Current. Alcohol. 5, 135–153.
Barnstable, C.J., Hofstein, R., Akagawa, K., 1985. A marker of early amacrine cell development in rat retina. Brain Res. 352, 286–290.
Bouskila, J., Burke, M.W., Zabouri, N., Casanova, C., Ptito, M., Bouchard, J.F., 2012. Expression and localization of the cannabinoid receptor type 1 and the enzyme fatty acid amide hydrolase in the retina of vervet monkeys. Neuroscience 202, 117–130.
Bouskila, J., Harrar, V., Javadi, P., Beierschmitt, A., Palmour, R., Casanova, C., Bouchard, J.F., Ptito, M., 2016a. Cannabinoid receptors CB1 and CB2 modulate the electroretinographic waves in vervet monkeys. Neural Plast. 2016, 1253245.
Bouskila, J., Harrar, V., Javadi, P., Casanova, C., Hirabayashi, Y., Matsuo, I., Ohyama, J., Bouchard, J.F., Ptito, M., 2016b. Scotopic vision in the monkey is modulated by the G protein-coupled receptor 55. Vis. Neurosci. 33, E006.
Bouskila, J., Javadi, P., Casanova, C., Ptito, M., Bouchard, J.F., 2013a. Muller cells express the cannabinoid CB2 receptor in the vervet monkey retina. J. Comp. Neurol. 521, 2399–2415.
Bouskila, J., Javadi, P., Casanova, C., Ptito, M., Bouchard, J.F., 2013b. Rod photoreceptors express GPR55 in the adult vervet monkey retina. PLoS One 8, e81080.
Bouskila, J., Javadi, P., Elkrief, L., Casanova, C., Bouchard, J.F., Ptito, M., 2016c. A comparative analysis of the endocannabinoid system in the retina of mice, tree shrews, and monkeys. Neural Plast. 2016, 3127658.
Bouskila, J., Javadi, P., Palmour, R.M., Bouchard, J.F., Ptito, M., 2014. Standardized full-field electroretinography in the green monkey (Chlorocebus sabaeus). PLoS One 9, e111569.
Brin, T., Borucki, K., Ambrosch, A., 2011. The influence of experimental alcohol load and alcohol intoxication on S100B concentrations. Shock 36, 356–360.
Brolese, G., Lunardi, P., Broetto, N., Engelke, D.S., Lirio, F., Batassini, C., Tramontina, A.C., Goncalves, C.A., 2014. Moderate prenatal alcohol exposure alters behavior and neuroglial parameters in adolescent rats. Behav. Brain Res. 269, 175–184.
Buckingham, T., Young, R., 1986. The rise and fall of intra-ocular pressure: the influence of physiological factors. Ophthalmic Physiol. Optic. 6, 95–99.
Burke, M., Zangenehpour, S., Bouskila, J., Boire, D., Ptito, M., 2009a. The gateway to the brain: dissecting the primate eye. JoVE, e1261.
Burke, M.W., Inyatkin, A., Ptito, M., Ervin, F.R., Palmour, R.M., 2016. Prenatal alcohol exposure affects progenitor cell numbers in olfactory bulbs and dentate gyrus of vervet monkeys. Brain Sci. 6.
Burke, M.W., Palmour, R.M., Ervin, F.R., Ptito, M., 2009b. Neuronal reduction in frontal cortex of primates after prenatal alcohol exposure. Neuroreport 20, 13–17.
Burke, M.W., Ptito, M., Ervin, F.R., Palmour, R.M., 2015. Hippocampal neuron populations are reduced in vervet monkeys with fetal alcohol exposure. Dev. Psychobiol. 57, 470–485.
Cecyre, B., Zabouri, N., Huppe-Gourgues, F., Bouchard, J.F., Casanova, C., 2013. Roles of cannabinoid receptors type 1 and 2 on the retinal function of adult mice. Invest. Ophthalmol. Vis. Sci. 54, 8079–8090.

Chan, T., Bowell, R., O'Keefe, M., Lanigan, B., 1991. Ocular manifestations in fetal alcohol syndrome. Br. J. Ophthalmol. 75, 524–526.
Chaudhuri, A., Zangenehpour, S., Matsubara, J.A., Cynader, M.S., 1996. Differential expression of neurofilament protein in the visual system of the vervet monkey. Brain Res. 709, 17–26.
Chmielewski, C.E., Hernandez, L.M., Quesada, A., Pozas, J.A., Picabea, L., Prada, F.A., 1997. Effects of ethanol on the inner layers of chick retina during development. Alcohol 14, 313–317.
Coles, C.D., 2011. Discriminating the effects of prenatal alcohol exposure from other behavioral and learning disorders. Alcohol Res. Health 34, 42–50.
Deng, J.X., Liu, X., Zang, J.F., Huang, H.E., Xi, Y., Zheng, H., Yao, H.L., Yu, D.M., Deng, J.B., 2012. The effects of prenatal alcohol exposure on the developmental retina of mice. Alcohol Alcohol 47, 380–385.
Donato, R., 2003. Intracellular and extracellular roles of S100 proteins. Microsc. Res. Tech. 60, 540–551.
Dursun, I., Jakubowska-Dogru, E., van der List, D., Liets, L.C., Coombs, J.L., Berman, R.F., 2011. Effects of early postnatal exposure to ethanol on retinal ganglion cell morphology and numbers of neurons in the dorsolateral geniculate in mice. Alcohol Clin. Exp. Res. 35, 2063–2074.
Evrard, S.G., Duhalde-Vega, M., Tagliaferro, P., Mirochnic, S., Caltana, L.R., Brusco, A., 2006. A low chronic ethanol exposure induces morphological changes in the adolescent rat brain that are not fully recovered even after a long abstinence: an immunohistochemical study. Exp. Neurol. 200, 438–459.
Evrard, S.G., Vega, M.D., Ramos, A.J., Tagliaferro, P., Brusco, A., 2003. Altered neuron-glia interactions in a low, chronic prenatal ethanol exposure. Brain Res. Dev. Brain Res. 147, 119–133.
Fakoya, F.A., 2005. Persistent neocortical astrogliosis in adult wistar rats following prenatal ethanol exposure. Brain Dev. 27, 259–265.
Fischer, A.J., Zelinka, C., Scott, M.A., 2010. Heterogeneity of glia in the retina and optic nerve of birds and mammals. PLoS One 5, e10774.
Hanson, J.W., Jones, K.L., Smith, D.W., 1976. Fetal alcohol syndrome. Experience with 41 patients. J. Am. Med. Assoc. 235, 1458–1460.
Harrar, V., Elkrief, L., Bouskila, J., Kucera, R., Fink-Jensen, A., Bouchard, J.F., Palmour, R., Ptito, M., 2017. Effects of prenatal alcohol exposure on the visual system of monkeys measured at different stages of development. Invest. Ophthalmol. Vis. Sci. 58, 6282–6291.
Hug, T.E., Fitzgerald, K.M., Cibis, G.W., 2000. Clinical and electroretinographic findings in fetal alcohol syndrome. J. AAPOS 4, 200–204.
Junemann, A.G., Rejdak, R., Huchzermeyer, C., Maciejewski, R., Grieb, P., Kruse, F.E., Zrenner, E., Rejdak, K., Petzold, A., 2015. Elevated vitreous body glial fibrillary acidic protein in retinal diseases. Graefes Arch. Clin. Exp. Ophthalmol. 253, 2181–2186.
Kashyap, B., Frederickson, L.C., Stenkamp, D.L., 2007. Mechanisms for persistent microphthalmia following ethanol exposure during retinal neurogenesis in zebrafish embryos. Vis. Neurosci. 24, 409–421.
Kim, I.B., Kim, K.Y., Joo, C.K., Lee, M.Y., Oh, S.J., Chung, J.W., Chun, M.H., 1998. Reaction of Muller cells after increased intraocular pressure in the rat retina. Exp. Brain Res. 121, 419–424.
Lantz, C.L., Pulimood, N.S., Rodrigues-Junior, W.S., Chen, C.K., Manhaes, A.C., Kalatsky, V.A., Medina, A.E., 2014. Visual defects in a mouse model of fetal alcohol spectrum disorder. Front Pediatr 2, 107.
Leske, M.C., Warheit-Roberts, L., Wu, S.Y., 1996. Open-angle glaucoma and ocular hypertension: the long island glaucoma case-control study. Ophthalmic Epidemiol. 3, 85–96.
Lewis, E.G., Dustman, R.E., Beck, E.C., 1970. The effects of alcohol on visual and somatosensory evoked responses. Electroencephalogr. Clin. Neurophysiol. 28, 202–205.
Malinow, M.R., Feeney-Burns, L., Peterson, L.H., Klein, M.L., Neuringer, M., 1980. Diet-related macular anomalies in monkeys. Invest. Ophthalmol. Vis. Sci. 19, 857–863.
Miller, M.W., Robertson, S., 1993. Prenatal exposure to ethanol alters the postnatal development and transformation of radial glia to astrocytes in the cortex. J. Comp. Neurol. 337, 253–266.
Murawski, N.J., Moore, E.M., Thomas, J.D., Riley, E.P., 2015. Advances in diagnosis and treatment of fetal alcohol spectrum disorders: from animal models to human studies. Alcohol Res 37, 97–108.
Papia, M.F., Burke, M.W., Zangenehpour, S., Palmour, R.M., Ervin, F.R., Ptito, M., 2010. Reduced soma size of the M-neurons in the lateral geniculate nucleus following foetal alcohol exposure in non-human primates. Exp. Brain Res. 205, 263–271.
Popova, S., Lange, S., Shield, K., Mihic, A., Chudley, A.E., Mukherjee, R.A.S., Bekmuradov, D., Rehm, J., 2016. Comorbidity of fetal alcohol spectrum disorder: a systematic review and meta-analysis. Lancet 387, 978–987.
Reeves, R.H., Yao, J., Crowley, M.R., Buck, S., Zhang, X., Yarowsky, P., Gearhart, J.D., Hilt, D.C., 1994. Astrocytosis and axonal proliferation in the hippocampus of S100b transgenic mice. Proc. Natl. Acad. Sci. U. S. A 91, 5359–5363.
Reichenbach, A., Stolzenburg, J.U., Eberhardt, W., Chao, T.I., Dettmer, D., Hertz, L., 1993. What do retinal muller (glial) cells do for their neuronal 'small siblings'? J. Chem. Neuroanat. 6, 201–213.
Renau-Piqueras, J., Zaragoza, R., De Paz, P., Baguena-Cervellera, R., Megias, L., Guerri, C., 1989. Effects of prolonged ethanol exposure on the glial fibrillary acidic protein-containing intermediate filaments of astrocytes in primary culture: a quantitative immunofluorescence and immunogold electron microscopic study. J. Histochem. Cytochem. 37, 229–240.
Riley, E.P., McGee, C.L., 2005. Fetal alcohol spectrum disorders: an overview with emphasis on changes in brain and behavior. Exp. Biol. Med. 230, 357–365.
Roozen, S., Black, D., Peters, G.Y., Kok, G., Townend, D., Nijhuis, J.G., Koek, G.H., Curfs, L.M., 2016. Fetal alcohol spectrum disorders (FASD): an approach to effective prevention. Curr Dev Disord Rep 3, 229–234.
Sáez, R., Burgal, M., Renau-Piqueras, J., Marqués, A., Guerri, C., 1991. Evolution of several cytoskeletal proteins of astrocytes in primary culture: effect of prenatal alcohol exposure. Neurochem. Res. 16, 737–747.
Sloane, J.A., Hollander, W., Rosene, D.L., Moss, M.B., Kemper, T., Abraham, C.R., 2000. Astrocytic hypertrophy and altered GFAP degradation with age in subcortical white matter of the rhesus monkey. Brain Res. 862, 1–10.
Sofroniew, M.V., 2009. Molecular dissection of reactive astrogliosis and glial scar formation. Trends Neurosci. 32, 638–647.
Sofroniew, M.V., Vinters, H.V., 2010. Astrocytes: biology and pathology. Acta Neuropathol. 119, 7–35.
Sofroniew, M.V., 2015. Astrocyte barriers to neurotoxic inflammation. Nat. Rev. Neurosci. 16, 249.
Stromland, K., 1985. Ocular abnormalities in the fetal alcohol syndrome. Acta Ophthalmol. Suppl. 171, 1–50.
Stromland, K., 1987. Ocular involvement in the fetal alcohol syndrome. Surv. Ophthalmol. 31, 277–284.
Stromland, K., Pinazo-Duran, M.D., 2002. Ophthalmic involvement in the fetal alcohol syndrome: clinical and animal model studies. Alcohol Alcohol 37, 2–8.
Sulik, K.K., Johnston, M.C., 1983. Sequence of developmental alterations following acute ethanol exposure in mice: craniofacial features of the fetal alcohol syndrome. Am. J. Anat. 166, 257–269.
Tanihara, H., Hangai, M., Sawaguchi, S., Abe, H., Kageyama, M., Nakazawa, F., Shirasawa, E., Honda, Y., 1997. Up-regulation of glial fibrillary acidic protein in the retina of primate eyes with experimental glaucoma. Arch. Ophthalmol. 115, 752–756.
Tenenbaum, A., Wexler, I., Merrick, J., 2016. Fetal alcohol syndrome. In: Rubin, I.L., Merrick, J., Greydanus, D.E., Patel, D.R. (Eds.), Health Care for People with Intellectual and Developmental Disabilities across the Lifespan. Springer International Publishing, Cham, pp. 873–880.
Tenkova, T., Young, C., Dikranian, K., Labruyere, J., Olney, J.W., 2003. Ethanol-induced apoptosis in the developing visual system during synaptogenesis. Invest. Ophthalmol. Vis. Sci. 44, 2809–2817.
Valles, S., Sancho-Tello, M., Minana, R., Climent, E., Renau-Piqueras, J., Guerri, C., 1996. Glial fibrillary acidic protein expression in rat brain and in radial glia culture is delayed by prenatal ethanol exposure. J. Neurochem. 67, 2425–2433.
Valles, S., Pitarch, J., Renau-Piqueras, J., Guerri, C., 1997. Ethanol exposure affects glial fibrillary acidic protein gene expression and transcription during rat brain development. J. Neurochem. 69, 2484–2493.
Vecino, E., Rodriguez, F.D., Ruzafa, N., Pereiro, X., Sharma, S.C., 2016. Glia-neuron interactions in the mammalian retina. Prog. Retin. Eye Res. 51, 1–40.
Volk, B., 1984. Cerebellar histogenesis and synaptic maturation following pre- and postnatal alcohol administration. An electron-microscopic investigation of the rat cerebellar cortex. Acta Neuropathol. 63, 57–65.
Walz, W., 2000. Role of astrocytes in the clearance of excess extracellular potassium. Neurochem. Int. 36, 291–300.
Wolin, L.R., Massopust Jr., L.C., 1967. Characteristics of the ocular fundus in primates. J. Anat. 101, 693–699.
Wu, S.Y., Leske, M.C., 1997. Associations with intraocular pressure in the Barbados eye study. Arch. Ophthalmol. 115, 1572–1576.